ACS Catalysis

Research Article

pubs.acs.org/acscatalysis

# Hydrodeoxygenation of Guaiacol over Ru(0001): A DFT Study

Cheng-chau Chiu,[†,‡,§] Alexander Genest,[†] Armando Borgna,[§] and Notker Rösch*[,†,‡]

[†]Institute of High Performance Computing, Agency for Science, Technology and Research, 1 Fusionopolis Way, #16-16 Connexis, Singapore 138632, Singapore

[‡]Department Chemie and Catalysis Research Center, Technische Universität München, 85747 Garching, Germany

[§]Institute of Chemical & Engineering Sciences, Agency for Science, Technology and Research, 1 Pesek Road, Jurong Island, Singapore 627833, Singapore

Supporting Information

**ABSTRACT:** The hydrodeoxygenation (HDO) of aromatic oxygenates over ruthenium was studied computationally on the model system guaiacol (2-methoxyphenol) on Ru(0001) using a DFT method. In addition to the adsorption geometries of the aromatic intermediates, the study focused on the energetics of elementary reaction steps that occur during the HDO of guaiacol. Bond scissions at the aliphatic side group were calculated to have barriers of at most 69 kJ mol$^{-1}$. In contrast, barriers for the cleavage of the aromatic bonds $C_{aryl}$–O were determined at more than 100 kJ mol$^{-1}$. On the basis of calculated energetics, a reaction pathway for the HDO of guaiacol is proposed in which first the methyl group of the methoxy moiety is removed to yield catecholate. Subsequently, the oxo groups are replaced by H, yielding first phenolate and, finally, benzene. For the removal of the first oxygen center of catecholate, a substantially lower barrier (106 kJ mol$^{-1}$) than for the $C_{aryl}$–O cleavage of phenolate (189 kJ mol$^{-1}$) was calculated. This is rationalized by the strained structure of adsorbed catecholate. The high barrier for the second $C_{aryl}$–O scission step is line with recent experiments that yield phenol as the main product of guaiacol HDO over Ru/C.

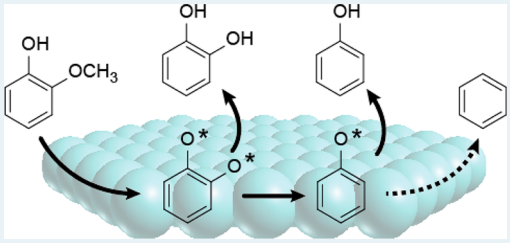


**KEYWORDS:** *guaiacol, ruthenium, hydrodeoxygenation, biomass, DFT*

## 1. INTRODUCTION

For the sustainable production of fuel, but also of other chemicals, pyrolysis of biomass has been shown to be a promising approach in the context of processing biomass.[1] The resulting "pyrolysis oil" contains a mixture of a large variety of oxygenate compounds.[2,3] For the intended purpose, the high oxygen content of this product mixture represents a problem as it is associated with undesired properties, e.g., chemical instability and low heating values.[4,5] Therefore, removal of oxygen functionalities is essential for increasing the quality of the pyrolysis oil and for compatibility with the current petrochemical infrastructure.[4]

One strategy for reaching these goals is hydrodeoxygenation (HDO)[6] in which formally the O containing groups are replaced by hydrogen atoms. Aromatic oxygenates, which mainly derive from the pyrolysis of lignin, have been shown to present a particular challenge because of the stability of the aromatic structures.[7] Various transition metals (TM) have been tested as catalysts for HDO of aromatics.[8−20] Among others, Ru, also known to display high selectivity for the formation of alkanes from aliphatic polyols,[21] has been shown to be a promising candidate.[18] For instance, guaiacol (2-methoxyphenol), a typical model molecule for aromatic pyrolysis products, has been reported to transform over Ru/C to phenol or benzene at temperatures between 250 and 400 °C.[10−13]

A rough idea about the mechanism for the HDO of aromatics on various (metallic and nonmetallic) catalysts including Ru can be gained from a large number of experiments, including isotope labeling, and the analysis of intermediate species as well as products observed under process conditions.[8,10,13,16,17,20,22−31] For instance, guaiacol HDO on Ru has been suggested to proceed via the intermediates catechol and phenol.[10] Nevertheless, the atomistic processes occurring at the catalyst surface remain unclear because computational studies dealing with aromatic oxygenates are not as numerous as those dealing with aliphatic oxygenates.[32] In particular, theoretical studies on aromatics on Ru surfaces are rare and limited to the adsorption of benzene[33] or larger aromatic hydrocarbons.[34] Recently, some computational results were communicated on reactions of complex substrates, such as guaiacol on Ru.[35] Computational studies for other metal surfaces are more abundant.[36] The adsorption of benzene on other close-packed surfaces was examined for TMs of groups 8,[37] 9,[38] 10,[38−48] and 11[48,49] as well as for alloys.[37] Reactions involving aromatics, e.g., the (de)hydrogenation[41,44,46,50−53] or the conversion of benzene to phenol,[47] have been computationally explored for surfaces of Rh, Ni, Pd, Pt, and Cu. The adsorption of aromatic oxygenates, such as phenol, anisole, cresol, or the more complex 1,3,5-trihydroxybenzene, have been the subject of computational studies on pure Fe,[54] Rh,[52]

Received: June 26, 2014
Revised: September 11, 2014
Published: October 23, 2014

   dx.doi.org/10.1021/cs500911j | ACS Catal. 2014, 4, 4178−4188

Ni,[40,53,54] Pd,[55] and Pt[43,52,55,56] surfaces as well as on surfaces of alloys such as FeNi[54] or FePd.[13]

Various computational works explicitly addressed the HDO of aromatics over metallic[35,54] and nonmetallic[57−59] catalysts. In many cases, the studies are limited to the adsorption of various model substrates on the catalyst surface.[54,57−59] However, a computational exploration of the reaction network is still missing, with the exception of some efforts.[35]

In the current work, we address calculated results for the HDO of guaiacol over large facets of Ru, modeled by a Ru(0001) surface. This surface is to be considered as a simplified model for Ru catalysts to explore the yet unknown potential energy surface for guaiacol HDO. The role of the surface structure of a "real" catalyst, which will contain defect sites, is not considered here. Thus, the results of this work should be understood as a first contribution to reveal the mechanism of the process under study. The present study does not address the quantitative decomposition of guaiacol into $C_1$ and $C_2$ fragments at 350 °C, which has been explored in only one set of experiments over Ru/C.[13]

## 2. COMPUTATIONAL MODELS AND METHODS

We carried out plane-wave-based DFT calculations on slab models using the program VASP (version 5.2.12),[60,61] employing the exchange-correlation functional PBE,[62,63] a generalized gradient approximation (GGA).[64] All calculations were carried out in spin-restricted fashion because spin moments of radicals are known to be quenched in complexes on Ru.[65] The electron−ion interaction was described by the projector-augmented wave method.[66,67] The cutoff energy was chosen at 400 eV. We invoked the first-order Methfessel−Paxton smearing technique[68] with a width of 0.1 eV and extrapolated the resulting energies to vanishing smearing width. For geometry optimizations, the Brillouin zone was sampled with a Monkhorst−Pack mesh[69] of 5 × 5 × 1 *k*-points; energies were evaluated in single-point fashion at the resulting geometries using a grid of 7 × 7 × 1 *k*-points. Appropriate dipole corrections were applied in all cases. The self-consistent field iterations were considered converged when the total energy changed by $<10^{-6}$ eV. For geometry optimization, the force on each relaxed atom was required to be $<2 \times 10^{-4}$ eV/pm.

To model the Ru(0001) surface, we used a slab of five close-packed Ru layers in a 5 × 5 hexagonal unit cell. The distance between repeated slabs was chosen to be more than 1.5 nm. The "top" two layers of each slab were relaxed while the other three Ru layers were kept at the optimized bulk geometry, with Ru−Ru = 270 pm. Molecular species in the gas phase were calculated using a cubic unit cell of 2 × 2 × 2 $nm^3$. The corresponding Brillouin zone was sampled at the Γ point only.

When searching for transition state (TS) structures, we first determined approximate structures with the nudged elastic band method[70,71] and the dimer method.[72] The resulting structures were subsequently refined using a quasi-Newton algorithm. All stationary points were verified by a normal-mode analysis.

We denote the surface adsorption complexes of the aromatic substrate species under study by labels **x**, **x** = **1**−**22** (Figures 1−3; Figure S1 of the Supporting Information, SI). Labels of the type $\mathbf{x}_{gp}$ denote the structure of adsorbate **x** in the gas phase. For small nonaromatic fragments, e.g., $OCH_x$ and $CH_x$, we refrained from introducing identifiers for ease of reading. Reactions from an initial state (IS) **x** to a product **y** (and a nonaromatic fragment) will be denoted as **x**−**y**; the corresponding TS as **x_y** (Figure 4; Figure S2 of SI). Cartesian coordinates of all stationary structures are provided as Supporting Information.

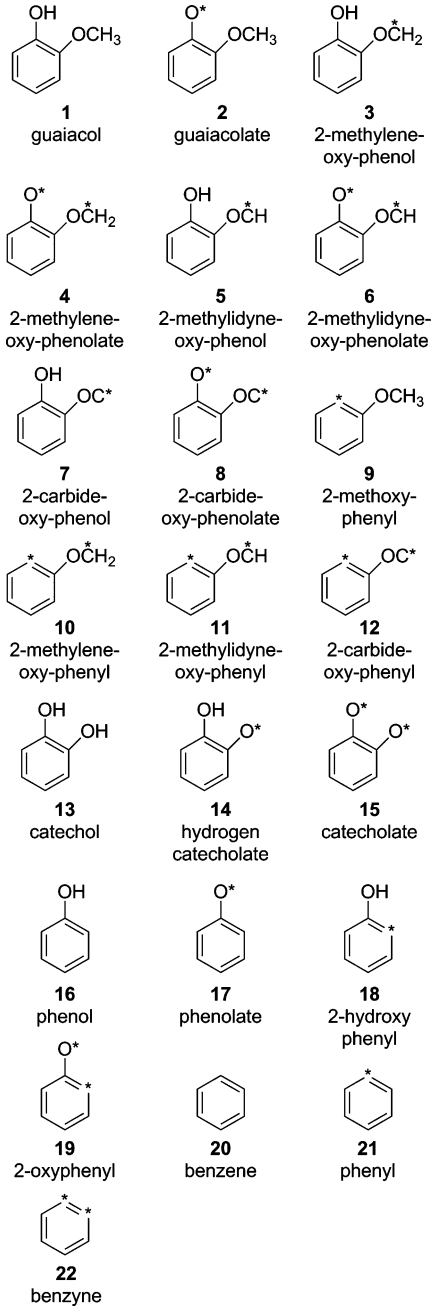


**Figure 1.** Schematic representation of the structures of reactants and intermediates under study. The structures are first sorted by the number of C atoms; then by the number of O atoms; and finally, by the number of H atoms. An asterisk indicates binding of a (di-) radical site to the metal surface.

Figures 1 and 2 provide an overview of all species and the reaction network under study. Table 1 shows calculated results of all surface reactions studied in the direction of the bond cleavage, although some of them may occur in the reverse direction along the reaction pathways to be discussed later on. For each reaction, we present the calculated reaction energy, $\Delta E_r = \Delta E(P) - \Delta E(IS)$, and activation barrier, $\Delta E_a = \Delta E(TS) - \Delta E(IS)$, with $\Delta E(IS)$, $\Delta E(TS)$, and $\Delta E(P)$ being the


dx.doi.org/10.1021/cs500911j | ACS Catal. 2014, 4, 4178−4188

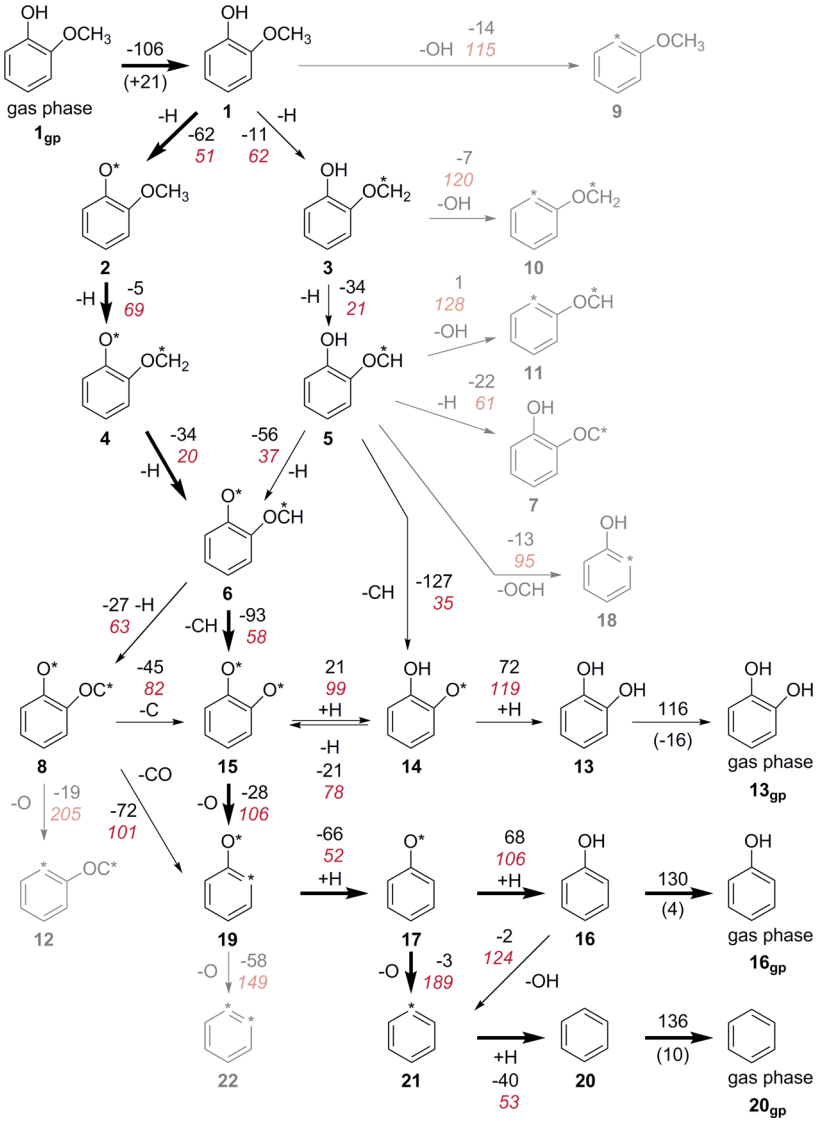


**Figure 2.** Schematic representation of the reaction pathways under study. Bold black arrows denote the main reaction pathway discussed in Section 3.3. The kinetically accessible alternative pathways are marked by thin black arrows. Numerical values at the arrows denote reaction energies (black, regular font) and activation barriers (red, italics) of the corresponding reaction steps. In addition, we show in gray other species examined that were determined not to be on a kinetically accessible pathway. Where appropriate, free energy values $\Delta G_{ads}$ or $\Delta G_{des}$ (400 °C, 1 bar) are shown in parentheses. Figure S7 of the SI provides an overview of the complete reaction network studied.

calculated absolute energies of the initial state, transition state, and product states, respectively. For the product state with coadsorbates **x** and **y**, we assume that the bond cleavage products are adsorbed at (formally) infinite separation, i.e., $\Delta E(\mathbf{x},\mathbf{y}) = \Delta E(\mathbf{x}) + \Delta E(\mathbf{y}) - \Delta E(\mathrm{Ru})$, where $\Delta E(\mathbf{x})$ and $\Delta E(\mathbf{y})$ represent the total energies of the adsorption complexes **x** and **y** on Ru and $\Delta E(\mathrm{Ru})$ is the total energy of the clean Ru(0001) surface.

In addition to energy values, we also provide the corresponding Gibbs free energies of reaction and activation, estimated according to standard procedures[73,74] as single-point corrections at pertinent experimental conditions[10−13] (250 °C, 400 °C; 1 bar, 40 bar total pressure).

## 3. RESULTS AND DISCUSSION

First, we discuss some structural aspects that are important for the reactivity. Subsequently, we will address energetic properties of pertinent elementary reactions to work out general trends of the reaction energies and the barriers. On the basis of these results, we finally will suggest the most likely reaction pathways.

**3.1. Adsorption Geometries.** The geometries of the adsorption complexes under study, discussed in detail in Section S1 of the SI, allowed us to identify preferred structural motifs regarding various functional groups of the adsorbates. In adsorption complexes of benzene **20** and other complexes with aromatic $C_6$ rings, the ring center is located over hollow sites (Figure 3), in agreement with the experimental structure of adsorbed benzene.[33,75,76] The C−O moiety of aromatic oxo groups (e.g., in the adsorption complex of phenolate **17**, Figure 3) also prefers to adsorb over a hollow site. In particular, the C center is close to a hollow site and the oxo group binds in top fashion to one of the Ru centers of the hollow site. A dehydrogenated aromatic C center (e.g., in the surface complex of phenyl **21**, Figure 3) is another frequent structural motif that prefers to adsorb over hollow sites.


dx.doi.org/10.1021/cs500911j | ACS Catal. 2014, 4, 4178−4188

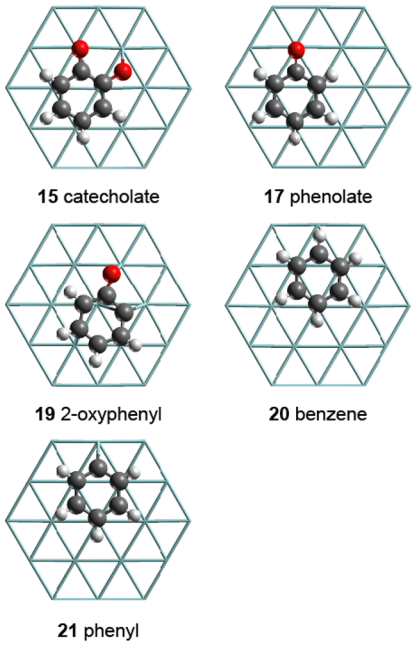


**Figure 3.** Optimized structures of selected local equilibrium configurations to illustrate the adsorption modes of reaction intermediates. For side views on these structures and further intermediate structures, see Figure S1 of the SI. Ru, cyan sticks; O, red; C, dark gray; H, white.

In some adsorption complexes, functional groups are unable to adsorb at their preferred adsorption sites. In the adsorption complex **15** of catecholate (Figure 3), one oxo group absorbs at the preferred top site, and the other one can be located only over an unfavorable bridge site or a skewed top site. The resulting unequal Ru−O distances of this bridge site, 231 and 245 pm, as well as the fact that the center of the aromatic ring is not directly above the center of a hollow site indicate that the adsorbate structure is under strain, as the two oxo groups and the aromatic ring compete for ideal adsorption sites. In addition, the C−O distances reflect strain in the adsorption complex **15**. The distances $C-O_{top}$ = 131 pm and $C-O_{bridge}$ = 135 pm indicate that the latter bond is more activated. Similarly, complex **19** experiences strain because the dehydrogenated C center and the oxo group compete for optimum sites. As the former adsorbs at a preferred hollow site, the C−O moiety of the oxo group is forced to align along a bridge site.

**3.2. Energetics of Reactions.** Next, we discuss the energy aspects, $\Delta E_r$ and $\Delta E_a$, of the reactions under study (Table 1). The reactions are grouped into six categories: bond cleavage of (i) O−H, (ii) $C_{alkyl}$−H, (iii) $C_{aryl}$−H, (iv) $C_{alkyl}$−O, (v) $C_{aryl}$−OH, and (vi) $C_{aryl}$−$OCH_x$.

*O−H Cleavage.* The dehydrogenation at the aromatic OH group has been studied for the species **1**, **3**, **5**, **13**, **14**, and **16**, which differ only in the substituent in the ortho position to the OH group. The corresponding reactions, **1**−**2**, **3**−**4**, **5**−**6**, **13**−**14**, **14**−**15**, and **16**−**17**, are all exothermic. With the exception of **14**−**15**, which will be discussed separately, all reactions feature similar energetics. The reaction energies, $\Delta E_r$, were

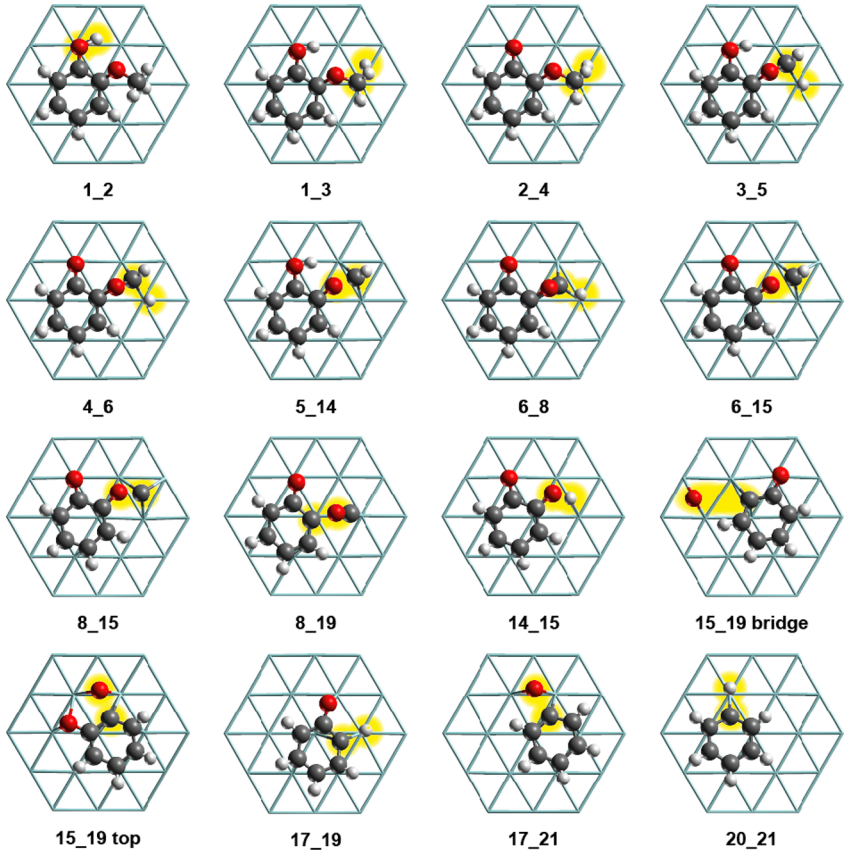


**Figure 4.** Optimized structures of transitions states along the most important pathways discussed in Section 3.3. For side views of these structures as well as TSs not shown here, see Figure S2 of the SI. Ru, cyan sticks; O, red; C, dark gray; H, white. The atoms associated with the bonds to be cleaved are highlighted.


dx.doi.org/10.1021/cs500911j | ACS Catal. 2014, 4, 4178−4188

Table 1. Calculated Reaction Energies, $\Delta E_r$, and Activation Barriers, $\Delta E_a$, of the Reactions under Study, Presented in the Direction of Bond Cleavage (kJ mol$^{-1}$)[a]

| | O−H | | | $C_{alkyl}$−H | | | $C_{aryl}$−H | | | $C_{alkyl}$−O | | | $C_{aryl}$−O(H) | | | $C_{aryl}$−OR | | |
|---|---|---|---|---|---|---|---|---|---|---|---|---|---|---|---|---|---|---|
| IS | P | $\Delta E_r$ | $\Delta E_a$ | P | $\Delta E_r$ | $\Delta E_a$ | P | $\Delta E_r$ | $\Delta E_a$ | P | $\Delta E_r$ | $\Delta E_a$ | P | $\Delta E_r$ | $\Delta E_a$ | P | $\Delta E_r$ | $\Delta E_a$ |
| **1** | **2**+H | −62 | 51 | **3**+H | −11 | 62 | | | | **14**+$CH_3$ | −104 | 171[b] | **9**+OH | −14 | 115 | **18**+$OCH_3$ | −33 | 102 |
| **2** | | | | **4**+H | −5 | 69 | | | | **15**+$CH_3$ | −64 | | **9**+O | −22 | 180 | **19**+$OCH_3$ | −7 | 143 |
| **3** | **4**+H | −55 | 49 | **5**+H | −34 | 21 | | | | **14**+$CH_2$ | −91 | 58 | **10**+OH | −7 | 120 | **18**+$OCH_2$ | −5 | 145 |
| **4** | | | | **6**+H | −34 | 20 | | | | **15**+$CH_2$ | −58 | 67 | **10**+O | −21 | 207 | **19**+$OCH_2$ | 15 | 168 |
| **5** | **6**+H | −55 | 37 | **7**+H | −22 | 61 | | | | **14**+CH | −127 | 35 | **11**+OH | 1 | 128 | **18**+OCH | −13 | 95 |
| **6** | | | | **8**+H | −27 | 63 | | | | **15**+CH | −93 | 58 | **11**+O | −13 | 177 | **19**+OCH | 7 | 107 |
| **8** | | | | | | | | | | **15**+C | −45 | 82 | **12**+O | −19 | 205 | **19**+CO | −72 | 101 |
| **13** | **14**+H | −72 | 47 | | | | | | | | | | | | | | | |
| **14** | **15**+H | −21 | 78 | | | | | | | | | | **19**+OH | 20 | 135 | | | |
| | | | | | | | | | | | | | **18**+O | −14 | 184 | | | |
| **15** | | | | | | | | | | | | | **19**+O | −28 | 106, 185 | | | |
| **16** | **17**+H | −68 | 37 | | | | | | | | | | **21**+OH | −2 | 124 | | | |
| **17** | | | | | | | **19**+H | 66 | 118 | | | | **21**+O | −3 | 189 | | | |
| **19** | | | | | | | | | | | | | **22**+O | −58 | 149 | | | |
| **20** | | | | | | | **21**+H | 40 | 92 | | | | | | | | | |

[a]Reactions are classified according to the categories introduced in Section 3.2. For each reaction, the initial state (IS) and the cleavage product (P) are listed; in some cases, various products have been examined. [b]Estimate; see Section S3 of the SI.

calculated in the range from −55 to −72 kJ mol$^{-1}$. The exothermicities of these reactions are related to the formation of a stable bond between an O functionality and an oxophilic metal, Ru. The corresponding reaction barriers were calculated at 37−51 kJ mol$^{-1}$, comparable to what has been reported for phenol on Rh(111).[52] Hence, these reactions can be considered as easily accessible under typical reaction conditions, 250−400 °C.[10−13] The reactions have in common that in the IS, the OH group does not interact with the Ru support (or does so only weakly), whereas the oxo group of the product adsorbs at a top site. These similarities in $\Delta E_r$ and $\Delta E_a$ values can be rationalized by the fact that the various substituents in the ortho position hardly affect the local structure around the OH group.

Reaction **14**−**15** has a higher barrier (78 kJ mol$^{-1}$) and is less exothermic (−21 kJ mol$^{-1}$) than the other OH cleavage steps. The different energetics of this reaction can be understood from the structure of product **15**. At variance with all other O−H cleavage steps discussed above, the O center of the OH group is forced to adsorb to an unfavorable bridge site upon dehydrogenation. This is related to the binding competition of the two oxo functionalities and the resulting structural strain in structure **15**; see Section 3.1.

The dehydrogenation barriers of OH substituents of aromatic compounds, discussed here, are slightly lower than those of aliphatic OH groups (42−78 kJ mol$^{-1}$).[77,78] In contrast, a direct comparison between the reaction energies of aromatic and aliphatic O−H cleavage steps is not straightforward. The values for the cleavage of aliphatic O−H groups scatter much stronger, from −22 to −64 kJ mol$^{-1}$,[76,77] than the values associated with the scission of aromatic O−H groups.

*$C_{alkyl}$−H Cleavage.* This category includes the dehydrogenation steps at the methoxy group. The reactions in this category can be divided into two groups. There is either a hydroxy group (**1**−**3**, **3**−**5**, **5**−**7**) in ortho position to the $OCH_x$ moiety ($x$ = 3−1) being dehydrogenated, or an oxo group (**2**−**4**, **4**−**6**, **6**−**8**). Similar to the O−H cleavage mechanism discussed above, the effect of the substituent in ortho position is limited. The values $\Delta E_r$ and $\Delta E_a$ of analogous reactions of the two groups agree within 7 kJ mol$^{-1}$. We find barriers of 62 (**1**−**3**) and 69 kJ mol$^{-1}$ (**2**−**4**) for the removal of the first H atom from the methoxy group. The corresponding reaction energies are slightly exothermic, −11 and −5 kJ mol$^{-1}$, respectively. Removal of the second hydrogen, **3**−**5** and **4**−**6**, is both kinetically and thermodynamically more favored, with $\Delta E_r$ = −34 kJ mol$^{-1}$ and $\Delta E_a \approx$ 20 kJ mol$^{-1}$. The third and last dehydrogenation steps yielding a −OC moiety (**5**−**7**, **6**−**8**) have barriers of 61 and 63 kJ mol$^{-1}$, respectively, which are comparable to those of the first dehydrogenation step **1**−**3** (62 kJ mol$^{-1}$) and **2**−**4** (69 kJ mol$^{-1}$). These reactions are also exothermic, by −22 and −27 kJ mol$^{-1}$, respectively.

The reaction energies presented here differ somewhat from those calculated for the dehydrogenation of ethanol on Ru(0001), for which the first dehydrogenation at the ethyl moiety is endothermic.[77] In contrast, the energies $\Delta E_r$ of the reactions at the methoxy group of guaiacol presented here resemble more the $\Delta E_r$ values reported for methane dehydrogenation, in which the first three dehydrogenation steps are also exothermic.[79−81] Note that the methoxy O center is not interacting with the Ru surface in any of the initial or product structures, whereas the O−Ru interaction plays an important role in the case of ethanol.[77] This may explain why the energetics of the reaction at the methoxy group of guaiacol resembles the reaction of methane, which does not contain any O.

The dehydrogenation barriers of the first dehydrogenation steps **1**−**3** and **2**−**4** at the methoxy group were calculated higher than those of the corresponding secondary dehydrogenation steps **3**−**5** and **4**−**6**, respectively. This ordering of the barriers can be rationalized by noting that in the initial states **1** and **2**, the methyl group interacts only weakly with the surface; hence, the methyl C−H bonds are essentially not activated. In contrast, the intermediates **3** and **4** bind notably to the catalyst. This argument is corroborated by results of computational studies on aliphatic substrates on Ru, for which the highest barriers were determined for the dehydrogenation of saturated C moieties.[77,80,82]

*$C_{aryl}$−H Cleavage.* The prototypical $C_{aryl}$−H cleavage reaction is the dehydrogenation **20**−**21** of adsorbed benzene to form adsorbed phenyl **21**. This transformation is


dx.doi.org/10.1021/cs500911j | ACS Catal. 2014, 4, 4178−4188

endothermic, $\Delta E_r$ = 40 kJ mol$^{-1}$, with a high barrier of 92 kJ mol$^{-1}$. Analogous reactions on other transition metal surfaces have been reported to be even more endothermic, 75 [Pt(111)[46]] and 71 kJ mol$^{-1}$ [Cu(100)[50]]; at least the latter reaction is kinetically hindered, $\Delta E_a$ = 179 kJ mol$^{-1}$.[50] Yet, the situation on Ru may be quite different from that on these late transition metals because the adsorption complex of the product phenyl shows noteworthy differences. As discussed in Section S1 of the SI, the phenyl moiety lies flat on the Ru(0001) surface (Structure **21** in Figure S1 of the SI) but is adsorbed upright or tilted on Pt and Cu surfaces. The second reaction in this category is reaction **17**−**19**; namely, the dehydrogenation in ortho position to the oxo group of phenolate. This reaction is both thermodynamically ($\Delta E_r$= 66 kJ mol$^{-1}$) and kinetically ($\Delta E_a$= 118 kJ mol$^{-1}$) less favored than **20**−**21** (Table 1). This can be rationalized by the structure of the product adsorption complex **19**, in which the substrate is under strain (Section 3.1).

*$C_{alkyl}$−O Cleavage.* This category of reactions comprises cleavage of the $H_xC$−O bond with $x$ = 1−3 (Table 1). In analogy to the $C_{alkyl}$−H cleavage reactions, these reactions can also be divided into two groups, recognizing that the ISs have either a hydroxyl substituent or an oxo group at the ring. While the latter group of reactions yields adsorbed catecholate **15** as product, the former group leads to the formation of the adsorption complex of hydrogen catecholate **14**.

We start with the latter groups of reactions yielding **14**. The bond scission barrier decreases with $x$, from 171 kJ mol$^{-1}$ estimated for **1**−**14** ($x$ = 3; see Section S3 of the SI) to 58 kJ mol$^{-1}$ for **3**−**14** ($x$ = 2) and 35 kJ mol$^{-1}$ for **5**−**14** ($x$ = 1). The corresponding reaction energy does not show such a clear trend as the barriers. Nevertheless, these reactions are generally strongly exothermic, with reaction energies ranging from −91 (**3**−**14**) to −127 kJ mol$^{-1}$ (**5**−**14**). The analogous reaction energies for the group yielding catecholate **15** are generally less exothermic, by 33−40 kJ mol$^{-1}$ (Table 1). This difference is related to the two oxo groups of the product structure **15** competing for the optimum adsorption site; see Section 3.1. In line with the less exothermic $\Delta E_r$ values for the reactions of the oxo-substituted ISs, the barriers of **4**−**15** and **6**−**15** are also higher than those of the reactions of the OH-substituted reactants, by 9 (**3**−**14**) and 23 kJ mol$^{-1}$ (**5**−**14**). Reaction **2**−**15** was not considered because a barrier above $\Delta E_a$(**1**−**14**) = 171 kJ mol$^{-1}$ is expected. Similar to the reactions of the first group, the barriers decrease with $x$ in the O−$CH_x$ group. We also examined reaction **8**−**15**, the IS of which has no H at the aliphatic C center ($x$ = 0). For this reaction, we determined a barrier, $\Delta E_a$ = 82 kJ mol$^{-1}$, that is higher than the values calculated for reactions **4**−**15** and **6**−**15**. Obviously, the barriers of $C_{alkyl}$−O cleavage do not fall synchronously with the decreasing number $x$ of H substituents at the O−$CH_x$ group; there is a minimum at $x$ = 1 instead. A similar trend with a minimum has also been found for the C−O cleavage barriers of ethanol and its dehydrogenation products on Ru(0001).[77]

*$C_{aryl}$−O(H) Cleavage.* The removal of an oxo or a hydroxyl group from the aromatic systems under study is generally characterized by barriers higher than 100 kJ mol$^{-1}$ (Table 1). With the exceptions of the reactions **15**−**19** and **19**−**22**, which we will address separately, a clear trend can be observed. Cleavage reactions of $C_{aryl}$−OH bonds generally exhibit barriers from 115 kJ mol$^{-1}$ to 135 kJ mol$^{-1}$, whereas removal of an oxo group is kinetically even less favored, with barriers from 177 to 207 kJ mol$^{-1}$. In contrast, thermodynamics tends to prefer the removal of an oxo group over the elimination of an OH group. Removal of an oxo group is always calculated to be exothermic, with $\Delta E_r$ values from −3 to −22 kJ mol$^{-1}$. On the other hand, the analogous removal of an OH group from an O-hydrogenated intermediate is, in all cases where our data allow a direct comparison, less exothermic or even endothermic (Table 1).

Reaction **15**−**19** is a special case as the IS surface complex of catecholate features two oxo groups, where one is adsorbed at a top; the other, at a bridge site. The barrier associated with the removal of the top-adsorbed O is 185 kJ mol$^{-1}$, comparable to values found for other oxo removal steps (**2**−**9**, **4**−**10**, **6**−**11**, **8**−**12**, **14**−**18**, **17**−**21**) where the pertinent oxygen center is also attached to a top site. In contrast, the barrier associated with O adsorbed at the bridge site is significantly lower, 106 kJ mol$^{-1}$. Obviously, the adsorption site of the oxo group to be eliminated notably affects the barrier height, a consequence of the stronger activation of the C−$O_{bridge}$ resulting from the strain in the adsorbate structure (Section 3.1).

The second special case, **19**−**22**, is the only transformation that starts from an adsorption complex with a dehydrogenated C center in the $C_6$ ring, again a structure under strain. The product benyzne **22** is the only adsorption complex of this study where the $C_6$ moiety is oriented upright on the metal surface (Section S1 of SI). The reaction energy of −58 kJ mol$^{-1}$, and the barrier of 149 kJ mol$^{-1}$ indicates that this reaction is thermodynamically and kinetically more favorable than the oxo removal steps discussed above, **2**−**9**, **4**−**10**, **6**−**11**, **8**−**12**, **14**−**18**, and **17**−**21**. Obviously, reaction **19**−**22** is not comparable to these oxo-removal steps.

*$C_{aryl}$−OR Cleavage.* Comparable to the $C_{aryl}$−O(H) cleavage just discussed, this category of reactions also features rather high barriers, with $\Delta E_a$ values from 95 kJ mol$^{-1}$ to 168 kJ mol$^{-1}$. After all, the cleavage of any $C_{aryl}$−O bond is kinetically challenging, irrespective of the substitution pattern at the oxygen. Similar to the $C_{alkyl}$−O cleavage, the substituent in the position ortho to the $OCH_x$ group of the IS has a notable effect on the energetics.

For OH group in ortho position, one yields intermediate **18** as the product of slightly exothermic reactions, with $\Delta E_r$ from −5 to −33 kJ mol$^{-1}$. The corresponding barriers fall into the range from 95 to 145 kJ mol$^{-1}$. Neither reaction energies nor barriers show a clear trend with the number of H centers at the aliphatic C, but the highest barrier is associated with the least exothermic reaction **3**−**18**, where R = $CH_2$. The reactions of the intermediates, which have an oxo group instead of the OH groups, yield **19** as the product. Compared with the reactions yielding **18**, these reactions are generally less favored in terms of both the reaction energy and the activation barrier. The values of $\Delta E_a$ for these reactions range from 101 to 168 kJ mol$^{-1}$; they are higher by at least 12 kJ mol$^{-1}$ than the barriers of the reactions from the corresponding O-hydrogenated ISs. With the exception of reaction **8**−**19**, these reactions are either slightly exothermic, $\Delta E_r$(**2**−**19**) = −7 kJ mol$^{-1}$, or slightly endothermic. Reaction **8**−**19** is a rather exothermic reaction, −72 kJ mol$^{-1}$; note that it involves the formation of the stable side product CO. The general energetic preference for reactions of intermediates with an OH group over the reactions of their O-dehydrogenated analogues is, similar to the cases of $C_{alkyl}$−O cleavage, due to the competition between the oxo group and the "bare" C moiety in the product structure **19** for the optimum structure of the resulting adsorption complex.


dx.doi.org/10.1021/cs500911j | ACS Catal. 2014, 4, 4178−4188

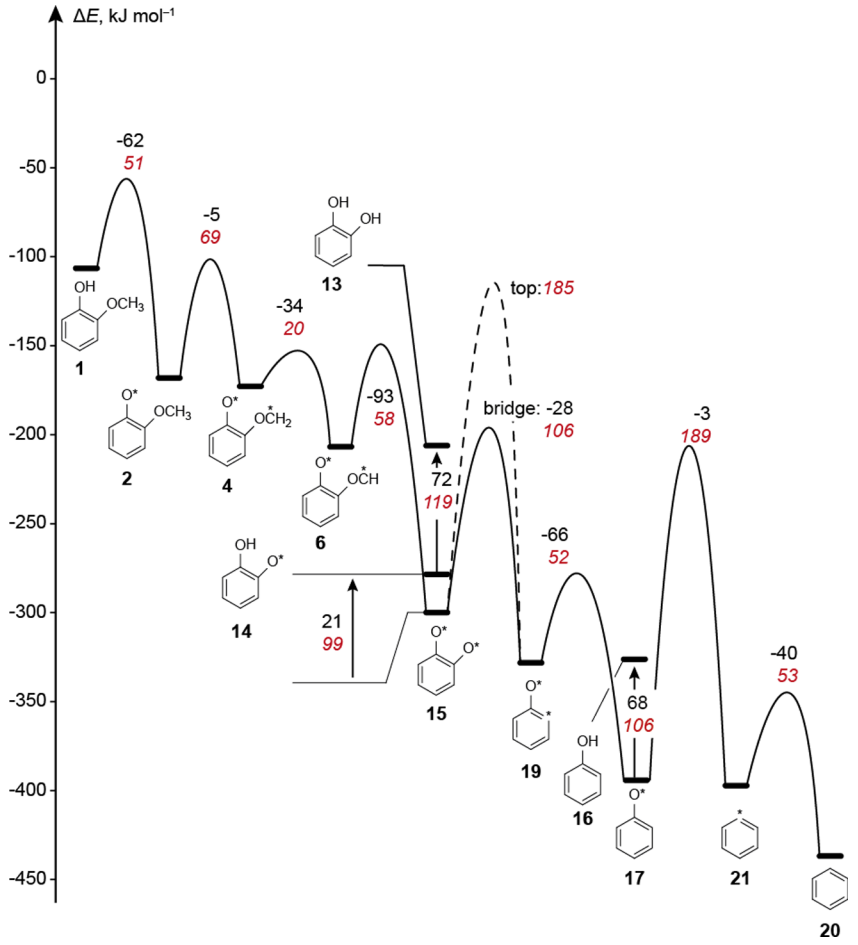


**Figure 5.** Energy profile of the most likely reaction pathway. Intermediate states are represented by bars; TS states, by arches. Numerical values at the arcs denote reaction energies (black, regular font) and activation barriers (red, italics) of the corresponding reaction steps. The dashed arc marks the barrier of an unfavorable C−O cleavage in **15** where the O center is at a top site. Also shown are reaction energies and barriers of hydrogenation steps that yield nonradical intermediates.

**3.3. Reaction Pathways.** Now we will present possible pathways that can be deduced from the energy properties of the reactions presented in the preceding section. We will start with the most likely pathway (Figures 2 and 5), which has been derived choosing for each intermediate the reaction with the lowest activation barrier. Subsequently, we will discuss alternative pathways (Figure 2; Figures S5 and S6 of the SI) that involve reaction barriers that are slightly higher (typically by up to 10 kJ mol$^{-1}$) than those encountered along the most likely pathway. The TSs involved in the pathways discussed here are displayed in Figure 4.

*The Most Likely Pathway.* Starting from gas phase guaiacol $\mathbf{1}_{gp}$ and a clean Ru surface with large facets, modeled by Ru(0001), the first step of this pathway is the exothermic formation of the adsorption complex of guaiacol **1** on the metal surface. The energy change associated with this step is −107 kJ mol$^{-1}$. For adsorption complex **1**, we determined only two reactions with $\Delta E_a$ < 100 kJ mol$^{-1}$: the exothermic dehydrogenation of the OH group (**1**−**2**, $\Delta E_a$ = 51 kJ mol$^{-1}$) and of the methyl group (**1**−**3**, $\Delta E_a$ = 62 kJ mol$^{-1}$). The most likely transformation is the formation of the surface complex of guaiacolate **2**, which stabilizes the system by −62 kJ mol$^{-1}$. However, this is not the most exothermic reaction of **1**. In the most exothermic reaction of **1**, the removal of the methyl group (**1**−**14**) with $\Delta E_r$ = −104 kJ mol$^{-1}$, a high barrier, estimated at ∼170 kJ mol$^{-1}$, has to be overcome. After the dehydrogenation at the hydroxyl group, the most likely pathway continues with two consecutive exothermic dehydrogenation steps at the methyl group, **2**−**4** and **4**−**6**, with barriers of 69 and 20 kJ mol$^{-1}$, respectively. All other reactions studied of the intermediate **2** can be ruled out as possible side reactions because their barriers were determined to at least 143 kJ mol$^{-1}$.

The dehydrogenation **2**−**4** at the methyl group activates the bonds at the aliphatic functionality in the product **4**. This is reflected not only in the low barrier for the further dehydrogenation as just mentioned, but also in the barrier for the cleavage reaction **4**−**15** of the $CH_2$−O bond, 67 kJ mol$^{-1}$. For comparison, recall the high barrier, estimated at 171 kJ mol$^{-1}$ for the scission step **1**−**14** of the $CH_3$−O bond, before the methyl C is dehydrogenated. All barriers of all cleavage reactions of type $C_{aryl}$−O in **4** were calculated far above 100 kJ mol$^{-1}$ (Table 1).

The most likely pathway leads from **4** to intermediate **6** where, again, the reactions with the lowest barriers are related to **6**−**8**, the removal of the (last) H of the aliphatic carbon center, $\Delta E_a$ = 63 kJ mol$^{-1}$, and the cleavage **6**−**15** of the $C_{alkyl}$−O bond, $\Delta E_a$ = 58 kJ mol$^{-1}$. All other transformations of intermediate **6** are unlikely in view of their significantly higher barriers, at least 107 kJ mol$^{-1}$. There is another pathway, via the intermediates **3** and **5**, for forming **6**; see below when


dx.doi.org/10.1021/cs500911j | ACS Catal. 2014, 4, 4178−4188

alternative pathways are being discussed. In **6**, for the first time along this pathway, the barriers of $C_{alkyl}$−H and $C_{alkyl}$−O bond scission of an intermediate are comparable. In view of the slightly lower barrier of $C_{alkyl}$−O scission, accompanied by a significantly stronger exothermicity, $\Delta E_r$ = −93 kJ mol$^{-1}$, we consider transformation **6**−**15** yielding catecholate as the more likely next reaction. The alternative pathway continuing with the less exothermic dehydrogenation step **6**−**8**, $\Delta E_r$ = −27 kJ mol$^{-1}$, will be discussed later on.

For adsorbed catecholate **15**, two alternatives have to be considered as consecutive reactions: rehydrogenation **15**−**14** (reversed **14**−**15**) at one O site and cleavage **15**−**19** of the $C_{aryl}$−O bond. The two reactions have comparable barriers: 99 and 106 kJ mol$^{-1}$, respectively. The hydrogenation step is endothermic by 21 kJ mol$^{-1}$, whereas the C−O cleavage step is exothermic by −28 kJ mol$^{-1}$. After a second endothermic hydrogenation step with a high barrier (reversed **13**−**14**, $\Delta E_r$ = 72 kJ mol$^{-1}$, $\Delta E_a$ = 119 kJ mol$^{-1}$) and the endothermic desorption step ($\Delta E_{des}$ = 116 kJ mol$^{-1}$), the rehydrogenation path ultimately leads to the formation of catechol $\mathbf{13}_{gp}$ in the gas phase (Figures 2 and 5), the first intermediate observed in experiment over Ru/C.[10] In the following, we will not consider the formation of adsorbed catechol **13** from adsorbed catecholate **15** as part of the main pathway because the overall process is rather endothermic.

More likely seems the C−O cleavage **15**−**19** to form 2-oxyphenyl on the surface **19**, for which we considered two consecutive reactions. Intermediate **19** can either be rehydrogenated at the aromatic ring (reverse **17**−**19**) to form the aromatic adsorption complex of phenolate **17** or undergo a second C−O cleavage step **19**−**22** to form benzyne. The reaction energies of both transformations are comparable: $\Delta E_r$(**19**−**17**) = −66 kJ mol$^{-1}$, $\Delta E_r$(**19**−**22**) = −58 kJ mol$^{-1}$. However, the activation barriers are significantly different: $\Delta E_a$(**19**−**17**) = 52 kJ mol$^{-1}$, $\Delta E_a$(**19**−**22**) = 149 kJ mol$^{-1}$. Therefore, formation of benzyne **22** is kinetically ruled out.

Adsorbed phenolate **17** is a very stable species that renders any transformation a challenge. The hydrogenation of **17** at O is endothermic (reverse **16**−**17**), with $\Delta E_r$ = 68 kJ mol$^{-1}$ and $\Delta E_a$ = 106 kJ mol$^{-1}$. Desorption of the resulting phenol yielding $\mathbf{16}_{gp}$ is endothermic by 130 kJ mol$^{-1}$. The situation is similar to that of catecholate, for which, overall, 209 kJ mol$^{-1}$ is required to yield catechol $\mathbf{13}_{gp}$ in the gas phase from adsorbed catecholate. Here, the overall energetics is almost as energy-intensive, consuming 198 kJ mol$^{-1}$ to yield gas phase phenol $\mathbf{16}_{gp}$ by hydrogenation of adsorbed phenolate **17** and subsequent desorption of the adsorbate. However, unlike the C−O cleavage **15**−**19** of catecholate, the competing thermoneutral C−O cleavage **17**−**21** of phenolate has a very high barrier, 189 kJ mol$^{-1}$; hence, it is kinetically hindered.

Thus, the calculated results predict that the transformation of guaiacol over Ru(0001) ends at the stage of phenolate or phenol. This is consistent with the experiment over Ru/C carried out under low $H_2$ pressure, below 1 bar, where the main product indeed is phenol.[11−13] However, benzene is observed as the product under high $H_2$ pressure, ∼40 bar.[10] Therefore, we will also include the further reaction of the C−O cleavage product phenyl **21** to benzene **20** in the current discussion, despite the high barrier for forming **21**. The final step from phenyl to benzene is the exothermic rehydrogenation **21**−**20** (reversed **20**−**21**) at the ring, $\Delta E_r$ = −40 kJ mol$^{-1}$, which has a barrier of 53 kJ mol$^{-1}$. Consistent with the desorption of guaiacol, catechol, and phenol, desorption of the final product benzene is a strongly endothermic process, requiring 136 kJ mol$^{-1}$.

In view of the high barrier of the C−O cleavage **17**−**21** of phenolate, we also considered the possibility that phenolate is hydrogenated to form phenol (reverse **16**−**17**) before the C−O bond cleaves to yield phenyl and OH in reaction **16**−**21**, which has a barrier of 124 kJ mol$^{-1}$ (Figure S4 in the SI). Yet, the highest lying TS along this pathway, **16_21**, is less stable by 192 kJ mol$^{-1}$ than the surface complex of phenolate **17**. TS **16_21** is of comparable stability to TS **17_21** which is less stable by 189 kJ mol$^{-1}$ than structure **17**. Thus, the C−O cleavage mechanism via TS **16_17** is as unfavorable as the "direct" scission of the C−O bond via reaction **17**−**21**.

The energy of phenol $\mathbf{16}_{gp}$ in the gas phase is less stable by 9 kJ mol$^{-1}$ than TS **17_21** (Figure 5). Thus, the experiments[10−13] showing the desorption of phenol cannot be rationalized by the calculated value $\Delta E_{des}$ of phenol. This discrepancy can be resolved by considering entropy effects. Pertinent free energies of desorption $\Delta G_{des}$ are significantly lower than the corresponding desorption energies $\Delta E_{des}$ (Table 2). For phenol, $\Delta E_{des}$ = 130 kJ mol$^{-1}$, whereas $\Delta G_{des}$ is at most 48 kJ mol$^{-1}$ (at 250 °C, 40 bar). Thus, phenol, but similarly also catechol and benzene (Table 2), can easily desorb. Indeed, all three species have been detected in the gas phase.[10−13]

**Table 2. Calculated Energies $\Delta E_{des}$ and Gibbs Free Energies $\Delta G_{des}$ Associated with the Desorption of Relevant Adsorbates (kJ mol$^{-1}$)**

| | | | $\Delta G_{des}$ | | | |
|---|---|---|---|---|---|---|
| | | $\Delta E_{des}$ | 250 °C 1 bar | 250 °C 40 bar | 400 °C 1 bar | 400 °C 40 bar |
| **1** | guaiacol | 107 | 7 | 23 | −21 | 0 |
| **13** | catechol | 116 | 14 | 30 | −16 | 5 |
| **16** | phenol | 130 | 32 | 48 | 4 | 25 |
| **20** | benzene | 136 | 37 | 53 | 10 | 30 |

The overall reaction path presented is consistent with the mechanism formulated by Laurent and Delmon originally proposed for the reaction over the alloys CoMo and NiMo[8] and recently also suggested for the reaction on Ru.[10] The present exploration elaborated details of the reactions at the surface. Indeed, the $C_{alkyl}$−O bond cleaves before the two $C_{aryl}$−O are consecutively cleaved; however, the cleavage steps do not occur from guaiacol, catechol, and phenol, as originally proposed,[8] but from their dehydrogenated analogues. These significantly more stable intermediates are radicaloid surface species that are unable to desorb and thus cannot be detected in the product mixture. Another aspect, not covered in the original mechanism,[8] is the activation of the methoxy group before the $C_{alkyl}$−O cleavage step. The carbon center is not removed as a methyl group because the cleavage of the C−O bond is kinetically accessible only after the $CH_3$ group has been dehydrogenated, which allows a bond to be formed between the C center and the catalyst surface, hence leading to an activated $C_{alkyl}$−O bond.

*Alternative Pathways.* As mentioned above, as an initial step, guaiacol does not necessarily have to be dehydrogenated at the OH group (**1**−**2**), leading to an alternative path for forming intermediate **6**. The dehydrogenation step **1**−**3** at the methoxy group is also feasible (Figure 2 and Figure S5 of the SI) because the corresponding barrier is higher than that of the **1**−**2** step by only 11 kJ mol$^{-1}$. Similar to the most likely


dx.doi.org/10.1021/cs500911j | ACS Catal. 2014, 4, 4178−4188

pathway, the methoxy group is activated by the removal of the first H, as just discussed. The methoxy group continues to dehydrogenate (**3**−**5**), exposing an O−CH moiety in intermediate **5**. The energy profile of the reactions from **1** to **5** (Figure S5 of SI) is comparable to the profile from **2** to **6** discussed for the most likely pathway (Figures 2, 5). Corresponding values of $\Delta E_a$ and $\Delta E_r$ differ by, at most, 7 kJ mol$^{-1}$. Intermediate **5** may undergo two further reactions. One option is the dehydrogenation **5**−**6** at the OH group, yielding **6** (Figure 2, Figure S5 of SI), an intermediate on the most likely pathway. The highest barrier along when forming **6** via **3** and **5** is 62 kJ mol$^{-1}$, even slightly lower than the highest barrier, 69 kJ mol$^{-1}$, on the most likely path. However, the first reaction, **1**−**2**, of the most likely pathway is 51 kJ mol$^{-1}$ more exothermic than the initial step **1**−**3** of the alternative pathway discussed here. As a consequence, the stationary points along the main path are always more stable than the stationary points along the alternative path (Figure S5 of SI).

The second kinetically accessible reaction for **5** is the bond scission **5**−**14** of $C_{alkyl}$−O, which is strongly exothermic, $\Delta E_r$ = −127 kJ mol$^{-1}$, and its barrier, 35 kJ mol$^{-1}$, is comparable to that of **5**−**6**. As discussed in Section 3.2, this reaction is both thermodynamically and kinetically more favored than the analogous reaction **6**−**15**, which is part of the most likely pathway. As a result of the lower barrier for **5**−**14**, the competing reaction **5**−**7**, the removal of the last H from the original methoxy group is unlikely to occur, which is different from the most likely pathway, because the barrier $\Delta E_a$(**5**−**7**) is not reduced compared with the analogous reaction **6**−**8** of the OH-dehydrogenated species. Reaction **5**−**7** requires an activation energy of 61 kJ mol$^{-1}$, comparable to **6**−**8**.

A similar reaction path was proposed in a recent computational study addressing HDO of guaiacol over Ru.[35] There, species **5** is assumed to form as discussed here.[35] Then, instead of proceeding with the scission of the $C_{alkyl}$−O bond **5**−**14** as done here, cleavage of the $C_{aryl}$−O bond **5**−**18** was suggested to occur with a calculated barrier of 102 kJ mol$^{-1}$,[35] slightly higher than our value of 95 kJ mol$^{-1}$. Recall that we ruled out reaction **5**−**18** because of the significantly lower barrier, only 35 kJ mol$^{-1}$, calculated for the competing reaction **5**−**14**.

As discussed in the context of the most likely pathway, the surface complex of hydrogen catecholate **14** obtained from C−O bond scission either can be hydrogenated at the oxo group to form catechol **13**, or it can dehydrogenate at the remaining OH group to from catecholate **15**, an intermediate of the main pathway.

Along the most likely pathway, in addition to guaiacol **1**, there is a second intermediate that does not have a clearly preferred reaction. For intermediate **6**, there are two reactions with similar barriers: the cleavage step **6**−**15** of $C_{alkyl}$−O, as discussed for the main pathway, and the less exothermic removal of the last H from the aliphatic carbon center, reaction **6**−**8** (Figure 2 and Figure S6 of SI). We will continue here with intermediate **8** for which three reactions have been considered. The kinetically most favored reaction, **8**−**15**, is the cleavage of the $C_{alkyl}$−O bond with $\Delta E_a$ = 82 kJ mol$^{-1}$ and $\Delta E_r$ = −45 kJ mol$^{-1}$. This alternative path and the most likely path differ only in the precursor of the $C_{alkyl}$−O cleavage, intermediate **6** with the moiety −OCH or intermediate **8** with the moiety −OC. Experiment could help with discriminating the two variants only if the surface species were analyzed.

Another reaction considered for **8** is the cleavage reaction **8**−**19** of the $C_{aryl}$−OC bond, which is 27 kJ mol$^{-1}$ more exothermic than **8**−**15** but requires overcoming a rather high activation barrier of 101 kJ mol$^{-1}$. This less likely route would lead to the direct formation of intermediate **19**, which also occurs in the most likely pathway, but without the preceding formation of the surface complex of catecholate **15** or its O-hydrogenated analogues **13** or **14**. The higher barrier calculated for this route is consistent with the experimental observation of catechol as an intermediate, demonstrating that the reaction pathway via the reaction **8**−**19** plays only a subordinate role. The third reaction for intermediate **8**, the removal of the oxo group in reaction **8**−**12**, can be easily ruled out for its high barrier of 205 kJ mol$^{-1}$.

Three of the four alternative pathways (Figures S5, S6 of SI) are very similar to the main path, differing only in radicaloid intermediates on the surface. Thus, experiments focusing on the analysis of products in the gas phase[10] cannot assist with confirming or rejecting these pathways

Finally, we note that for the present system, $\Delta G$ corrections are crucial only for adsorption/desorption processes. In contrast, energies and activation barriers of reactions on the surface are only slightly affected by free energy corrections; for further details, see Section S6 of the SI.

## 4. CONCLUSIONS

In this computational study, we proposed a reaction pathway for the hydrodeoxygenation of guaiacol over a Ru catalyst with large facets, using Ru(0001) as the model surface. According to our computational model, the reactions at the aliphatic methoxy side group of guaiacol follow patterns similar to those discussed in a previous work on ethanol on Ru(0001).[77] The $C_{alkyl}$−O bond is activated upon dehydrogenation at the $C_{alkyl}$ center and can be cleaved with barriers as low as 35 kJ mol$^{-1}$. This result allows one to rationalize why the primary product of guaiacol HDO on Ru around 400 °C is catechol.[10,11] It is plausible to assume that the formation of catechol from guaiacol in experiment on Pt[12,13,16,17,20] follows a similar mechanism. Recall that the activation of a $C_{alkyl}$−O upon dehydrogenation at the carbon center has also been reported for Pt.[83,84] In contrast to the $C_{alkyl}$−O bond, the $C_{aryl}$−O bonds have quite high cleavage barriers, above 100 kJ mol$^{-1}$, despite the aromatic C center being, per definition, unsaturated. Thus, the cleavage of the aromatic $C_{aryl}$−O bonds is the crucial step for the complete catalytic HDO of guaiacol.

We calculated the barriers for cleaving the aromatic $C_{aryl}$−O bonds to depend notably on the local environment of the $C_{aryl}$−O bond. When the corresponding oxo center is adsorbed at a top site, activation energies of more than 170 kJ mol$^{-1}$ are required. In contrast, the $C_{aryl}$−O bond with O adsorbed at a bridge site, as in the adsorption complex of catecholate, can be cleaved by overcoming a notably lower barrier of 106 kJ mol$^{-1}$. This reduced barrier is related to the fact that the adsorbed catecholate molecule, its bridge adsorbed oxo group in particular, is under strain because the functional groups of catecholate compete for optimum adsorption sites on the Ru(0001) surface. The dependence of the barriers on the local geometry indicates that the surface structure of the catalyst can play an important role for the HDO activity, a circumstance that may be exploited when designing a new catalyst.

Because our model does not consider coadsorbed hydrogen atoms on the surface, the presented calculations can be understood as a model for experiments at low $H_2$ pressure. In fact, our results, indicating that the phenolate C−O bond is difficult to cleave, agree well with the experiment at below 1 bar

$H_2$ over Ru/C[11−13] where one observes phenol as main product. Thus, despite the model character of our calculations, we were able to reveal important aspects of the HDO mechanism of guaiacol on Ru particles with large facets. However, HDO is a complex process, and experiments at ∼40 bar $H_2$ yield benzene as the main product instead of phenol,[10] indicating that significant effects on the selectivity may be induced by small changes of the process setup. It is desirable to explore how such changes of the experimental conditions affect the reactions at the molecular level to improve our understanding of HDO of aromatics. However, this is beyond the scope of the present work.

For a better understanding of the complete reaction network, an analysis of the kinetics based on the calculated data will be beneficial. In view of the complexity of the HDO process, such modeling (e.g., microkinetic simulations or kinetic Monte Carlo simulations) will be left to future work.

## ■ ASSOCIATED CONTENT

### Supporting Information

Discussion of structures of adsorption complexes, structures of all stationary points not shown in the main text, a comment on the calculation of the TS structure **1_14**, energetic profiles of alternative HDO pathways, absolute energies of intermediate and transition states of the discussed HDO pathways, Gibbs free energies of reaction and of activation for all surface reactions, Cartesian coordinates of all stationary points. This material is available free of charge via the Internet at http://pubs.acs.org.

## ■ AUTHOR INFORMATION

### Corresponding Author

*E-mail: roesch@mytum.de.

### Notes

The authors declare no competing financial interest.

## ■ ACKNOWLEDGMENTS

C.-c.C. is grateful for a fellowship by the International Graduate School of Science and Engineering at Technische Universität München and a scholarship from the A*STAR Research Attachment Program provided by the A*STAR Graduate Academy. This work was supported by generous allotments of computational resources at Leibniz Rechenzentrum München and the A*STAR Computational Resource Centre.

## ■ REFERENCES

(1) Anex, R. P.; Aden, A.; Kazi, F. K.; Fortman, J.; Swanson, R. M.; Wright, M. M.; Satrio, J. A.; Brown, R. C.; Daugaard, D. E.; Platon, A.; Kothandaraman, G.; Hsu, D. D.; Dutta, A. *Fuel* **2010**, *89* (Supplement 1), S29−S35.
(2) Mohan, D.; Pittman, C. U.; Steele, P. H. *Energy Fuels* **2006**, *20*, 848−889.
(3) Huber, G. W.; Iborra, S.; Corma, A. *Chem. Rev.* **2006**, *106*, 4044−4098.
(4) Resasco, D. E.; Crossley, S. *AIChE J.* **2009**, *55*, 1082−1089.
(5) Mortensen, P. M.; Grunwaldt, J. D.; Jensen, P. A.; Knudsen, K. G.; Jensen, A. D. *Appl. Catal., A* **2011**, *407*, 1−19.
(6) Elliott, D. C. *Energy Fuels* **2007**, *21*, 1792−1815.
(7) Ben, H.; Mu, W.; Deng, Y.; Ragauskas, A. J. *Fuel* **2013**, *103*, 1148−1153.
(8) Laurent, E.; Delmon, B. *Appl. Catal., A* **1994**, *109*, 97−115.
(9) Mortensen, P. M.; Grunwaldt, J.-D.; Jensen, P. A.; Jensen, A. D. *ACS Catal.* **2013**, *3*, 1774−1785.
(10) Chang, J.; Danuthai, T.; Dewiyanti, S.; Wang, C.; Borgna, A. *ChemCatChem* **2013**, *5*, 3041−3049.
(11) Boonyasuwat, S.; Omotoso, T.; Resasco, D.; Crossley, S. *Catal. Lett.* **2013**, *143*, 783−791.
(12) Gao, D.; Schweitzer, C.; Hwang, H. T.; Varma, A. *Ind. Eng. Chem. Res.* **2014**, DOI: 10.1021/ie500495z.
(13) Sun, J.; Karim, A. M.; Zhang, H.; Kovarik, L.; Li, X. S.; Hensley, A. J.; McEwen, J.-S.; Wang, Y. *J. Catal.* **2013**, *306*, 47−57.
(14) Lee, C. R.; Yoon, J. S.; Suh, Y.-W.; Choi, J.-W.; Ha, J.-M.; Suh, D. J.; Park, Y.-K. *Catal. Commun.* **2012**, *17*, 54−58.
(15) Elliott, D. C.; Hart, T. R. *Energy Fuels* **2008**, *23*, 631−637.
(16) Nimmanwudipong, T.; Aydin, C.; Lu, J.; Runnebaum, R.; Brodwater, K.; Browning, N.; Block, D.; Gates, B. *Catal. Lett.* **2012**, *142*, 1190−1196.
(17) Nimmanwudipong, T.; Runnebaum, R. C.; Block, D. E.; Gates, B. C. *Energy Fuels* **2011**, *25*, 3417−3427.
(18) Wildschut, J.; Mahfud, F. H.; Venderbosch, R. H.; Heeres, H. J. *Ind. Eng. Chem. Res.* **2009**, *48*, 10324−10334.
(19) Yakovlev, V. A.; Khromova, S. A.; Sherstyuk, O. V.; Dundich, V. O.; Ermakov, D. Y.; Novopashina, V. M.; Lebedev, M. Y.; Bulavchenko, O.; Parmon, V. N. *Catal. Today* **2009**, *144*, 362−366.
(20) Runnebaum, R. C.; Nimmanwudipong, T.; Block, D. E.; Gates, B. C. *Catal. Sci. Technol.* **2012**, *2*, 113−118.
(21) Davda, R. R.; Shabaker, J. W.; Huber, G. W.; Cortright, R. D.; Dumesic, J. A. *Appl. Catal., B* **2003**, *43*, 13−26.
(22) Ben, H.; Ferguson, G. A.; Mu, W.; Pu, Y.; Huang, F.; Jarvis, M.; Biddy, M.; Deng, Y.; Ragauskas, A. J. *Phys. Chem. Chem. Phys.* **2013**, *15*, 19138−19142.
(23) Wan, H.; Chaudhari, R. V.; Subramaniam, B. *Top. Catal.* **2012**, *55*, 129−139.
(24) Jin, S.; Xiao, Z.; Li, C.; Chen, X.; Wang, L.; Xing, J.; Li, W.; Liang, C. *Catal. Today* **2014**, *234*, 125−132.
(25) Bykova, M. V.; Ermakov, D. Y.; Kaichev, V. V.; Bulavchenko, O. A.; Saraev, A. A.; Lebedev, M. Y.; Yakovlev, V. A. *Appl. Catal., B* **2012**, *113−114*, 296−307.
(26) Bui, V. N.; Toussaint, G.; Laurenti, D.; Mirodatos, C.; Geantet, C. *Catal. Today* **2009**, *143*, 172−178.
(27) Zhao, C.; He, J.; Lemonidou, A. A.; Li, X.; Lercher, J. A. *J. Catal.* **2011**, *280*, 8−16.
(28) Ohta, H.; Kobayashi, H.; Hara, K.; Fukuoka, A. *Chem. Commun.* **2011**, *47*, 12209−12211.
(29) Girgis, M. J.; Gates, B. C. *Ind. Eng. Chem. Res.* **1991**, *30*, 2021−2058.
(30) He, Z.; Wang, X. *Catal. Sustain. Energy* **2012**, *1*, 28−53.
(31) Furimsky, E. *Catal. Today* **2013**, *217*, 13−56.
(32) Guo, N.; Caratzoulas, S.; Doren, D. J.; Sandler, S. I.; Vlachos, D. G. *Energy Environ. Sci.* **2012**, *5*, 6703−6716.
(33) Held, G.; Braun, W.; Steinrück, H.-P.; Yamagishi, S.; Jenkins, S.; King, D. *Phys. Rev. Lett.* **2001**, *87*, 216102.
(34) Lu, Y. H.; Zhang, H. J.; Xu, Y. F.; Song, B.; Li, H. Y.; Bao, S. N.; He, P. *Appl. Surf. Sci.* **2006**, *253*, 2025−2030.
(35) Lu, J.; Heyden, A. *Theoretical Study of the Liquid-phase Deoxygenation of Guaiacol into Aromatic Chemicals over Ru Surfaces.* At 23rd North American Catalysis Society Meeting, Louisville, Kentucky, USA, **2013**. https://nam.confex.com/nam/2013/webprogram/Paper7915.html (accessed June 11, 2014).
(36) Jenkins, S. J. *Proc. R. Soc. A* **2009**, *465*, 2949−2976.
(37) Hensley, A. J. R.; Zhang, R.; Wang, Y.; McEwen, J.-S. *J. Phys. Chem. C* **2013**, *117*, 24317−24328.
(38) Morin, C.; Simon, D.; Sautet, P. *J. Phys. Chem. B* **2004**, *108*, 5653−5665.
(39) Yamagishi, S.; Jenkins, S. J.; King, D. A. *J. Chem. Phys.* **2001**, *114*, 5765−5773.
(40) Delle Site, L.; Alavi, A.; Abrams, C. F. *Phys. Rev. B* **2003**, *67*, 193406.
(41) Mittendorfer, F.; Hafner, J. *J. Phys. Chem. B* **2002**, *106*, 13299−13305.
(42) Mittendorfer, F.; Hafner, J. *Surf. Sci.* **2001**, *472*, 133−153.

(43) Bonalumi, N.; Vargas, A.; Ferri, D.; Baiker, A. *J. Phys. Chem. B* **2006**, *110*, 9956−9965.
(44) Morin, C.; Simon, D.; Sautet, P. *Surf. Sci.* **2006**, *600*, 1339−1350.
(45) Saeys, M.; Reyniers, M.-F.; Marin, G. B.; Neurock, M. *J. Phys. Chem. B* **2002**, *106*, 7489−7498.
(46) Saeys, M.; Reyniers, M.-F.; Neurock, M.; Marin, G. B. *J. Phys. Chem. B* **2003**, *107*, 3844−3855.
(47) Orita, H.; Itoh, N. *Appl. Catal., A* **2004**, *258*, 17−23.
(48) Schravendijk, P.; van der Vegt, N.; Delle Site, L.; Kremer, K. *ChemPhysChem* **2005**, *6*, 1866−1871.
(49) Bilić, A.; Reimers, J. R.; Hush, N. S.; Hoft, R. C.; Ford, M. J. *J. Chem. Theory Comput.* **2006**, *2*, 1093−1105.
(50) Lesnard, H.; Bocquet, M.-L.; Lorente, N. *J. Am. Chem. Soc.* **2007**, *129*, 4298−4305.
(51) Saeys, M.; Reyniers, M. F.; Neurock, M.; Marin, G. B. *J. Phys. Chem. B* **2004**, *109*, 2064−2073.
(52) Honkela, M. L.; Bjork, J.; Persson, M. *Phys. Chem. Chem. Phys.* **2012**, *14*, 5849−5854.
(53) Ghiringhelli, L. M.; Caputo, R.; Delle Site, L. *Phys. Rev. B* **2007**, *75*, 113403.
(54) Nie, L.; de Souza, P. M.; Noronha, F. B.; An, W.; Sooknoi, T.; Resasco, D. E. *J. Mol. Catal. A: Chem.* **2014**, *388*−*389*, 47−55.
(55) Yang, J.; Dauenhauer, P. J.; Ramasubramaniam, A. *J. Comput. Chem.* **2013**, *34*, 60−66.
(56) Tan, Y. P.; Khatua, S.; Jenkins, S. J.; Yu, J. Q.; Spencer, J. B.; King, D. A. *Surf. Sci.* **2005**, *589*, 173−183.
(57) Badawi, M.; Paul, J.-F.; Cristol, S.; Payen, E. *Catal. Commun.* **2011**, *12*, 901−905.
(58) Moon, J.-S.; Kim, E.-G.; Lee, Y.-K. *J. Catal.* **2014**, *311*, 144−152.
(59) Badawi, M.; Paul, J.-F.; Payen, E.; Romero, Y.; Richard, F.; Brunet, S.; Popov, A.; Kondratieva, E.; Gilson, J.-P.; Mariey, L.; Travert, A.; Maugé, F. *Oil Gas Sci. Technol.* **2013**, *68*, 829−840.
(60) Kresse, G.; Hafner, J. *Phys. Rev. B* **1994**, *49*, 14251−14269.
(61) Kresse, G.; Furthmüller, J. *Comput. Mater. Sci.* **1996**, *6*, 15−50.
(62) Perdew, J. P.; Burke, K.; Ernzerhof, M. *Phys. Rev. Lett.* **1996**, *77*, 3865−3868.
(63) Perdew, J. P.; Burke, K.; Ernzerhof, M. *Phys. Rev. Lett.* **1997**, *78*, 1396−1396.
(64) The large adsorption energies of all species under study indicate predominantly covalent interactions. Hence, the GGA-type PBE functional is suitable in the current context.
(65) Hammer, B. *Phys. Rev. Lett.* **1999**, *83*, 3681−3684.
(66) Blöchl, P. E. *Phys. Rev. B* **1994**, *50*, 17953−17979.
(67) Kresse, G.; Joubert, D. *Phys. Rev. B* **1999**, *59*, 1758−1775.
(68) Methfessel, M.; Paxton, A. T. *Phys. Rev. B* **1989**, *40*, 3616−3621.
(69) Monkhorst, H. J.; Pack, J. D. *Phys. Rev. B* **1976**, *13*, 5188−5192.
(70) Mills, G.; Jónsson, H.; Schenter, G. K. *Surf. Sci.* **1995**, *324*, 305−337.
(71) Mills, G.; Jacobsen, K. W.; Jónsson, H. Nudged elastic band method for finding minimum energy paths of transitions. In *Classical and Quantum Dynamics in Condensed Phase Simulations*; World Scientific: Singapore, River Edge, NJ, 1998; pp 385−404.
(72) Henkelman, G.; Jónsson, H. *J. Chem. Phys.* **1999**, *111*, 7010−7022.
(73) McQuarrie, D. A.; SImon, J. D. *Molecular Thermondynamics*; University Science Books: Sausalito, 1999.
(74) Chang, C.-R.; Zhao, Z.-J.; Köhler, K.; Genest, A.; Li, J.; Rösch, N. *Catal. Sci. Technol.* **2012**, *2*, 2238−2248.
(75) Stellwag, C.; Held, G.; Menzel, D. *Surf. Sci.* **1995**, *325*, L379−L384.
(76) Braun, W.; Held, G.; Steinrück, H. P.; Stellwag, C.; Menzel, D. *Surf. Sci.* **2001**, *475*, 18−36.
(77) Chiu, C.-c.; Genest, A.; Rösch, N. *Top. Catal.* **2013**, *56*, 874−884.
(78) Sinha, N. K.; Neurock, M. *J. Catal.* **2012**, *295*, 31−44.
(79) Ciobîcă, I. M.; Frechard, F.; van Santen, R. A.; Kleyn, A. W.; Hafner, J. *J. Phys. Chem. B* **2000**, *104*, 3364−3369.
(80) Ciobîcă, I. M.; Frechard, F.; van Santen, R. A.; Kleyn, A. W.; Hafner, J. *Chem. Phys. Lett.* **1999**, *311*, 185−192.
(81) Herron, J. A.; Tonelli, S.; Mavrikakis, M. *Surf. Sci.* **2013**, *614*, 64−74.
(82) Ciobica, I. M.; van Santen, R. A. *J. Phys. Chem. B* **2002**, *106*, 6200−6205.
(83) Alcalá, R.; Mavrikakis, M.; Dumesic, J. A. *J. Catal.* **2003**, *218*, 178−190.
(84) Chiu, C.-c.; Genest, A.; Rösch, N. *ChemCatChem* **2013**, *5*, 3299−3308.